A Parameterization of the Microwave Land Surface Emissivity Between 19 and 100 GHz, Anchored to Satellite-Derived Estimates

Catherine Prigent, Elodie Jaumouillé, Frédéric Chevallier, and Filipe Aires

Abstract—Land surface emissivities have been calculated for Tropical Rainfall Measuring Mission (TRMM) Microwave Instrument (TMI), Special Sensor Microwave/Imager (SSM/I), and Advanced Microwave Sounder Unit-A conditions, for two months (July 2002 and January 2003) over the globe at the European Centre for Medium-Range Weather Forecasts, directly from satellite observations. From this data set, a parameterization of the microwave emissivities that account for frequency, incidence angle, and polarization dependences is proposed. It is anchored to climatological monthly mean maps of the emissivities at 19, 37, and 85 GHz, which are calculated from SSM/I. For each location and time of the year, it provides realistic first-guess estimates of the microwave emissivities from 19 to 100 GHz, for all scanning conditions. The results are compared to radiative transfer model estimates. The new estimates provide rms errors that are usually within 0.02, with the noticeable exception of snow-covered regions where the high spatial and temporal variabilities of the emissivity signatures are difficult to capture.

Index Terms—Emissivity, land surface, microwave.

I. INTRODUCTION

FOR A large range of applications, there is a need for land surface microwave emissivity estimates, for all observation angles and polarizations, for the whole globe. Surface-sensitive microwave channels from satellite-borne instruments contain some key information about surface temperature, lower troposphere temperature, cloud liquid water, and precipitating water. Accurate microwave land surface emissivities are essential to properly extract such information in 1-D retrievals or within complex 4-D data assimilation systems in Numerical Weather Prediction (NWP) centers. The interaction between microwave radiation and the land surface is complex, being dependent on a large number of highly variable surface characteristics, such as soil humidity and roughness, vegetation properties, or snow cover. An extensive body of research has been directed toward a better understanding of the mechanisms

responsible for the microwave emission of land surfaces, from field experiments (using ground-based [1] or airborne sensors [2]), from radiative transfer modeling [3], [4], and from emissivity estimates derived from satellite observations [5]–[7].

Field experiments, which are under controlled conditions, provide high temporal and spatial resolution of the surface emissivity and make it possible to analyze the effect of detailed surface processes on the surface emissivity (e.g., freeze–thaw cycle, leaf orientation, or rain effect). However, they are performed for a limited number of surface types, observed under specific conditions (frequency and incidence angle), and have a difficulty in encompassing the large spatial and temporal variability of the surfaces measured from satellites at a global scale.

Land surface emissivity models have been developed for the globe for various surface conditions encountered over the continents [4], [8], using different radiative transfer solutions depending on the surface characteristics. Model inputs are provided by a land surface model, such as the one in the Global Data Assimilation System of the National Center for Environmental Prediction (NCEP) [4]. For specific surfaces and regional applications, coupling of land surface outputs with a radiative model can be efficient [9]. However, even when assuming that a perfect land surface emissivity model exists, the inputs it will require on a global basis (e.g., soil composition, texture, humidity, or roughness, vegetation and snow characteristics) would not be easily available with the spatial resolution compatible with the satellite and with the required accuracy.

Global land surface emissivity maps have been produced directly from satellite observations. For instance, emissivity atlases are calculated from Special Sensor Microwave/Imager (SSM/I) measurements [5], [7], by removing the contribution of the atmosphere, clouds, rain, and the surface temperature, using ancillary data. The emissivities are estimated for SSM/I observation conditions, i.e., between 19 and 85 GHz at 53° incidence angle, and for both vertical and horizontal polarizations. Advanced Microwave Sounder Unit (AMSU) emissivities have also been calculated [6], [10]. However, these satellite estimates are limited to the observation conditions of the given satellite (frequency, incidence angle, and polarization). For a given period of time, AMSU only provides a limited number of over-passes of the same location with the same incidence angle and does not give access to the vertical and horizontal polarization information separately. In addition, direct calculation of the emissivities from satellite observations requires a large amount of ancillary information that is not always easily accessible.

Good cloud filtering and a reliable surface skin temperature are particularly needed.

In order to provide the community with land surface emissivity estimates for the globe for all observing conditions (incidence angles and polarizations) between 19 and 100 GHz, we propose to derive a parameterization of the frequency, angular, and polarization dependences of the emissivity, anchored on a reliable satellite-derived emissivity database. First, satellite-derived estimates of the land surface emissivities are calculated from Tropical Rainfall Measuring Mission (TRMM) Microwave Instrument (TMI), SSM/I, and AMSU-A observations, for two months (July 2002 and January 2003) for the globe to analyze the frequency, angular, and polarization dependences for the different land surface types. A parameterization of the emissivity frequency, angular, and polarization dependences is deduced for each surface type. This parameterization along with the previously calculated SSM/I emissivity climatology at 19, 37, and 85 GHz for both polarizations at 53° provides an emissivity estimate for all locations on Earth for each month of the year, for all the incidence angles and polarizations between 19 and 100 GHz. The results are compared with model outputs.

II. EMISSIVITY DATA SETS

For a comprehensive analysis of the emissivity variations with surface type, frequency, angle, and polarization, this study examines and compares several sources of land surface microwave emissivity estimates, including satellite-derived values and model results.

A. Satellite-Derived Emissivity Data Sets

1) SSM/I, TMI, and AMSU-A Emissivity Database: In order to examine the frequency, angular, and polarization dependences for the full range of possible land surface conditions, microwave emissivities have been calculated at the European Centre for Medium Range Weather Forecasts (ECMWF) for all continents for two contrasted months (July 2002 and January 2003) from the satellite measurements derived from the following three instruments that have different observing conditions: SSM/I, TMI, and AMSU-A.

The Special Sensor Microwave/Imager (SSM/I) onboard the Defense Meteorological Satellite Program (DMSP) polar orbiters observes the Earth twice daily at 19.35, 22.235, 37.0, and 85.5 GHz with both the vertical and horizontal polarizations, with the exception of the 22 GHz (vertical polarization only). The observing incidence angle is close to 53°, and the fields of view decrease with frequency, from 43×69 km to 13×15 km [11].

The TMI is similar to SSM/I, with the addition of a lower frequency channel, a tropical orbit, and a better spatial resolution. It measures the microwave radiation in the tropical region from $\sim 40°$ S to $\sim 40°$ N, at five frequencies, 10.65, 19.35, 21.30, 37.00, 85.50 GHz, for both the vertical and horizontal polarizations (except at the 21.30 GHz which is only observed in the vertical polarization). The incidence angle is $\sim 53°$. The spatial resolution ranges from 36.8×63.2 km at 10.65 GHz to 4.6×7.2 km at 85.50 GHz.

The AMSU-A onboard the NOAA polar orbiters provides atmospheric temperature profiling capabilities [12]. The window channels are at 23.8, 31.4, and 89 GHz. It is a cross-track scanning instrument, with 30 scan positions at 3.3° intervals from $-14.5 \times 3.3°$ to $+14.5 \times 3.3°$ which translate into local zenith angles θ_z up to 58.5°. The spatial resolution is 50 km at nadir. The polarization measured by AMSU-A rotates with the scan angle due to the rotating-reflector/fixed-feed type of antenna design and is a known mix of the vertical and horizontal polarizations (see [10] for more details).

The emissivity calculation method follows closely the scheme that was previously developed for SSM/I, which is described in detail in [5] and [7]. In this work, the selection of the clear pixels is based on the forecast model at ECMWF (not on the cloud flag from the International Satellite Cloud Climatology Project (ISCCP) [13] like in the previous work with SSM/I as this information is not available on real time to NWP centers). The observations that correspond to a nonzero fractional area cloud cover in the model are excluded. The atmospheric contribution is calculated from the ECMWF forecast model variables using the radiative transfer for the Tiros Operational Vertical Sounder (RTTOV) [14], [15].

An example of satellite-derived emissivity maps, which were calculated under clear-sky conditions and averaged over July 2002, is presented at 31.4 GHz from the AMSU-A observations for the incidence angles between 10° and 20° (Fig. 1). The holes in the maps correspond to the regions that are considered persistently cloudy during the month by the ECMWF forecast model.

2) Reference SSM/I-Derived Emissivity Database Over a Decade: The microwave land surface emissivities have been calculated over the globe for approximately ten years between 19 and 85 GHz at a 53° incidence angle for both vertical and horizontal polarizations using SSM/I observations. Ancillary data (ISCCP products [13] and NCEP reanalyses [16]) help remove the contribution from the atmosphere, clouds, and rain from the measured satellite signal and separate surface temperature from emissivity variations. This data set has been extensively evaluated (e.g., [7]), and in this study, it serves as a reference from which a monthly mean emissivity climatology is calculated and an emissivity-based surface-type classification is derived. This reference database is accessible at http://geo.obspm.fr/.

B. Model-Derived Emissivity Database

For comparison purposes, the emissivities have also been calculated at ECMWF, using the radiative transfer model from Weng *et al.* [4] with the forecast-model-relevant surface variables (soil temperature and humidity, vegetation fraction, and snow depth) as inputs. This model uses different solutions depending on the surface type.

III. ANALYSIS OF THE EMISSIVITY FREQUENCY AND ANGULAR DEPENDENCES

In order to facilitate the analysis of the frequency and angular dependences of the SSM/I, TMI, and AMSU emissivities, the data set is sorted per surface types. Instead of using an external
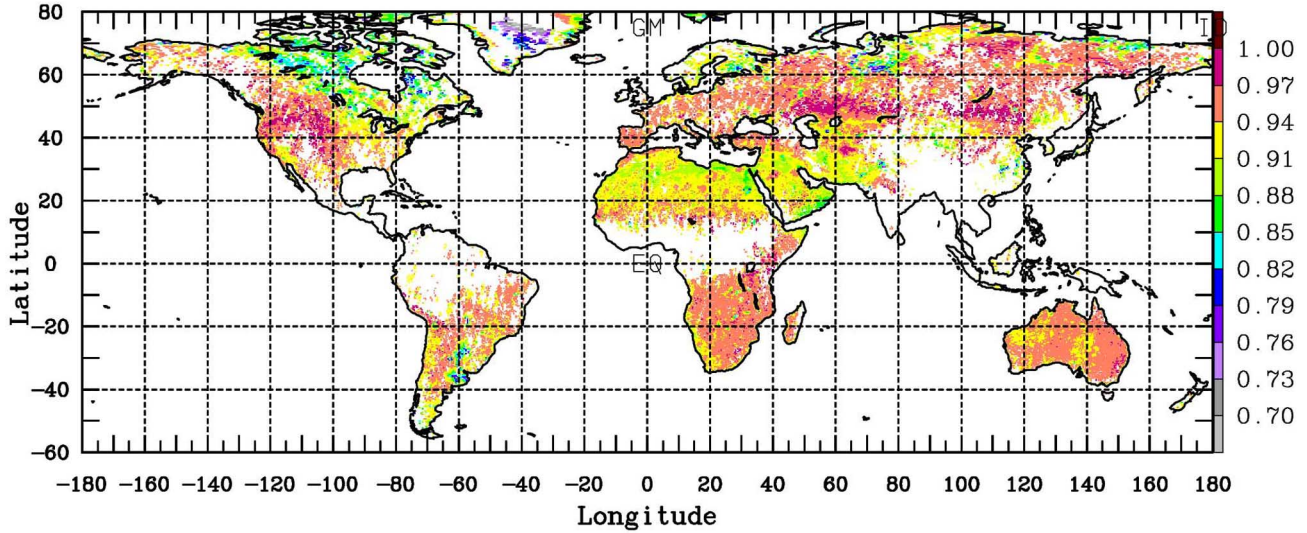
Fig. 1.　Satellite-derived emissivity from AMSU-A at 31.4 GHz for July 2002 for the incidence angles between $10°$ and $20°$.
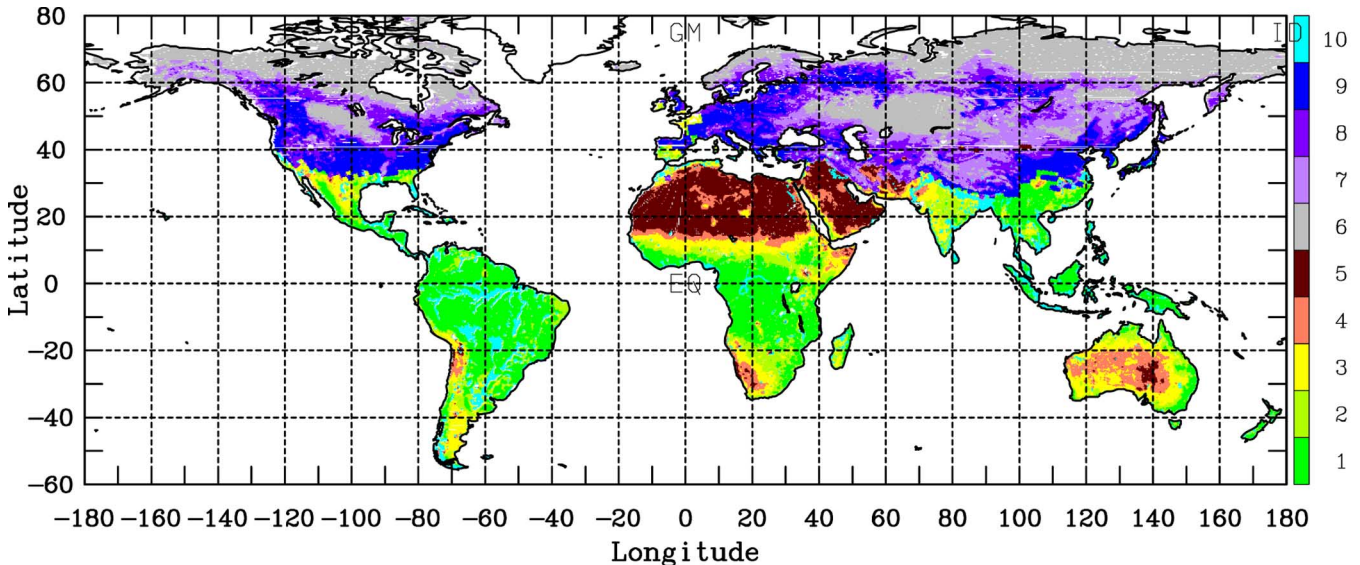

Fig. 2.　Result of the classification of SSM/I derived emissivities for January. Classes from 1 to 5 represent continental snow-free regions. Classes 6 to 9 correspond to snow-covered land, and pixels with standing water are grouped in class 10.

and independent classification of vegetation, we develop a classification of the SSM/I emissivity, based on the reference SSM/I emissivity data set: this insures that each class represents a different behavior in terms of microwave emissivities and that the set of classes describes the full variability of these emissivities. The frequency and angular dependences of the satellite-derived emissivities are then analyzed for each surface type and compared to the model ones.

A. Classification of the Emissivity Data Set

The monthly mean emissivity climatology is calculated from the decadal (1992–2001) SSM/I emissivity database. An unsupervised clustering technique is applied to this emissivity climatology for the seven SSM/I channels. The chosen classification scheme (topological method from [17]) imposes a neighborhood requirement on nearby classes so that results are

easier to interpret (for more details on the classification method, see [18]). The clustering method is applied twice as follows: once for the snow-free pixels, then for the snow-covered pixel (the snow and ice information is extracted from the National Snow and Ice Data Center; ice pixels are not considered). Five classes are isolated for the snow-free regions, corresponding to vegetation densities, from dense vegetation (class 1) to desert surfaces (class 5), and four snow classes are also determined. Pixels with more than 10% standing water are not considered in the clustering scheme and are grouped in class 10: it includes areas of rivers or lakes, as well as regions associated with seasonal wetlands as defined by [19]. Fig. 2 shows the result of the classification for the month of January applied to the reference data set. The snow-free classes (from 1 to 5) show consistent spatial structures related to vegetation density. Note that given the small number of classes considered here and the limited sensitivity of the passive microwave observations
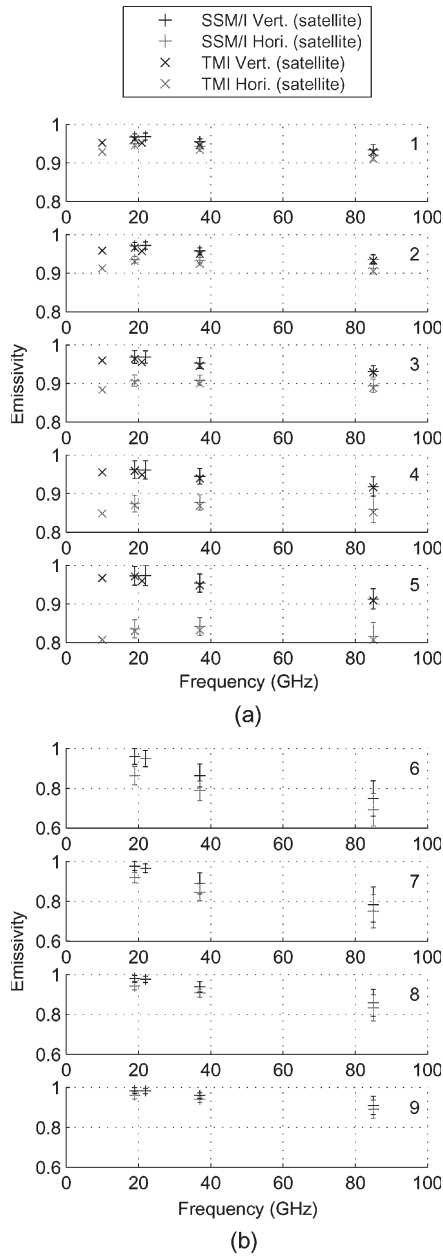
Fig. 3. Mean emissivity frequency dependence as observed from satellite-derived emissivities from the SSM/I and TMI at a 53° incidence angle, for both the vertical and horizontal polarizations for January 2003 (a) for the snow-free surface types and (b) for the snow-covered surfaces. The standard deviation is added for the SSM/I estimates.

at these frequencies to discriminate between very dense forest and moderate vegetation, most vegetated regions are grouped in classes 1 and 2. The snow classes as well present realistic structures, with class 6 related to dry and thick snow related to the strong scattering at 85 GHz, and class 9 associated to wet snow (see [20] for more details on the snow classification). We tried classifications with a higher number of classes, but this did not change significantly the final results of our analysis of the angular and frequency dependence of the emissivity. This basic classification was kept for this specific application. The same classification is then applied to the multisatellite two-month data set (SSM/I, TMI, and AMSU), based on the SSM/I emissivity values.
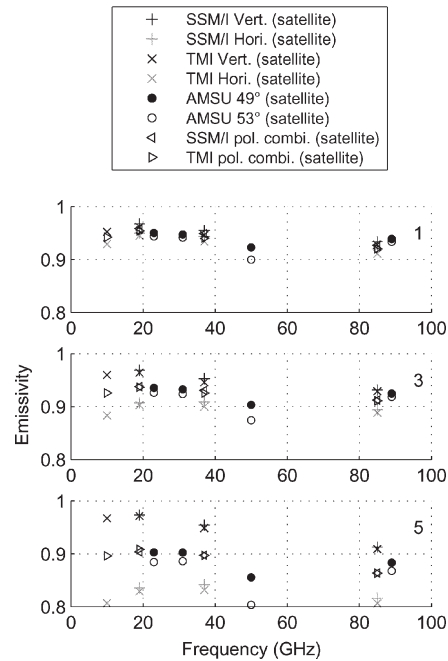

Fig. 4. Mean emissivity frequency dependence as observed from satellite-derived emissivities from the SSM/I, TMI, and AMSU-A around a 53° incidence angle for the three snow-free surface types. Both the vertical and horizontal polarizations are shown for the SSM/I and TMI. For AMSU-A, a polarization combination is measured, and for comparison, the same combination is calculated from the SSM/I and TMI perpendicular polarizations.

In the interpolation process, the emissivity of a specific location and month, for a given frequency, angle, and polarization, will be estimated from the actual emissivity of that location and month in the SSM/I-derived emissivity climatology, using the classification information only for the derivation of the frequency and angular dependences.

B. Frequency Dependence

1) Analysis With the Satellite-Derived Emissivities: The data set of two months of SSM/I, TMI, AMSU emissivities is sorted per surface types, using the SSM/I emissivity classification. For each snow-free class, Fig. 3(a) shows the frequency dependence of the SSM/I and TMI emissivity estimates in both polarizations, calculated from the satellite observations. The standard deviation over the class is indicated for the SSM/I estimates for each class. The results are shown for January 2003. The emissivities calculated from the satellite observations from SSM/I and TMI for the same frequencies agree very well for all the classes. The emissivities above 19 GHz have a very weak and close to linear frequency dependence, decreasing with frequencies, regardless of surface types. The TMI 21-GHz emissivity sticks out for all surface classes. It is likely related to an intercalibration problem. It could also be associated to a problem in the estimation of the absorption in the water vapor line, due to gaseous model errors or to errors in the water vapor profile estimates. This has not been elucidated. The 10-GHz emissivities are systematically and significantly lower than the 19-GHz ones, for both polarizations.

For the snow classes, Fig. 3(b) shows the frequency variation of the SSM/I emissivities (TMI does not cover the northern
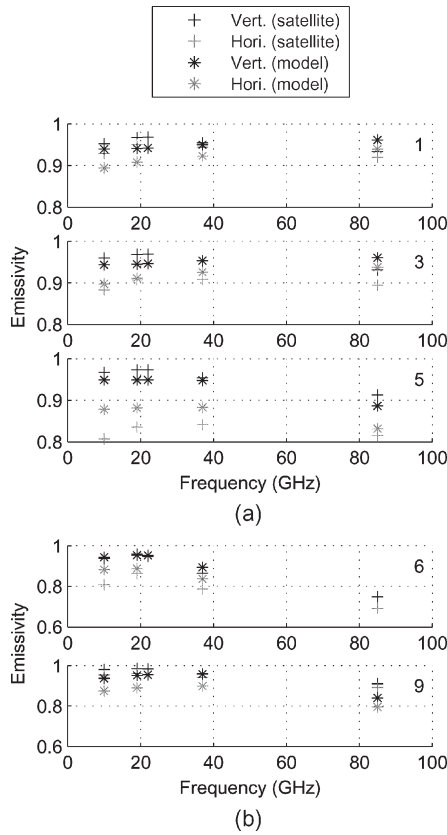
Fig. 5.   Mean emissivity frequency dependence as observed from satellite-derived emissivities and from a model simulation at a 53° incidence angle, for both polarizations for January 2003, (a) for the snow-free surface types and (b) for the snow-covered surfaces. The satellite-derived estimates are from the SSM/I at 19 GHz and above and from TMI at 10 GHz. A limited number of classes are shown, the intermediate ones having an intermediate behavior. Note that the model values for the second snow type are out of the plotted range (lower values).
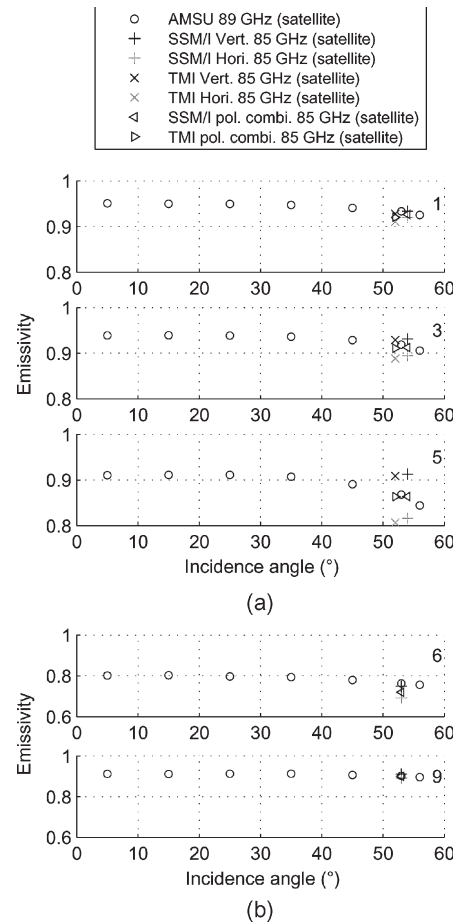

Fig. 6.   Mean emissivity angular dependence as observed from satellite-derived emissivities from AMSU-A at 85 GHz, as compared to the SSM/I and TMI estimates at a 53° incidence angle in January 2003 (a) for three snow-free surface types and (b) for snow types.

latitudes and, as a consequence, provides very limited snow-emissivity estimates). The emissivity decreases with frequency. The slope is stronger for class 6 which corresponds to the very cold regions where snow grains are likely large and can significantly scatter the microwave radiation. The higher the frequency, the stronger the scattering, thus explaining the decrease of the emissivities with frequency [20].

Fig. 4 compares the AMSU emissivities derived from the satellite observations to the SSM/I and TMI satellite-derived emissivities. The AMSU satellite emissivities over 4° around 53° are averaged for comparisons with TMI and SSM/I. In addition to the vertical and horizontal polarizations, the polarization combination that corresponds to the AMSU geometry is added. The satellite emissivity estimate at 50.3 GHz is obviously problematic, which is likely contaminated by error in the atmospheric correction (see [10] for additional comments on this problem). At low frequencies, the SSM/I- and TMI-derived emissivities are larger than the AMSU ones. However, above 80 GHz, the opposite prevails regardless of the surface type.

2) Comparison With Model Estimates: Fig. 5 compares the SSM/I emissivity estimates from the satellite observations and from the Weng *et al.* model [4]. The satellite estimates show a much larger polarization dependence than the model over arid and low-density vegetations [classes 5 and 4 on Fig. 5(a)], par-

ticularly at low frequencies. The following two reasons could explain it: the model can overestimate the roughness effect, or the assumed surface parameters are not adequate. Regardless of the surface type, the satellite-derived emissivities decrease with increasing frequency. Over the arid regions (class 5), the emissivities predicted by the model are rather stable with frequencies up to 40 GHz, and then decrease. Over the vegetated regions (classes from 1 to 3), the modeled emissivities increase with frequencies for the horizontal polarization. At 10 GHz with TMI, large differences are observed between the satellite estimates and the model, particularly for the horizontal polarization and over the arid regions.

For snow-covered regions, the differences between the satellite and model emissivities are significant but the trends in the frequencies are similar (note that the scales on the y-axis on Fig. 5(a) and (b) are different and that the model values for the snow type 6 at 85 GHz are lower than the plotted range).

C. Angular Dependence

The analysis of the angular dependence of the satellite data can only be performed from the AMSU-A observations, i.e., not independently for each polarization.

The AMSU-satellite emissivities at 89 GHz are shown for different angles on Fig. 6, along with the SSM/I and TMI
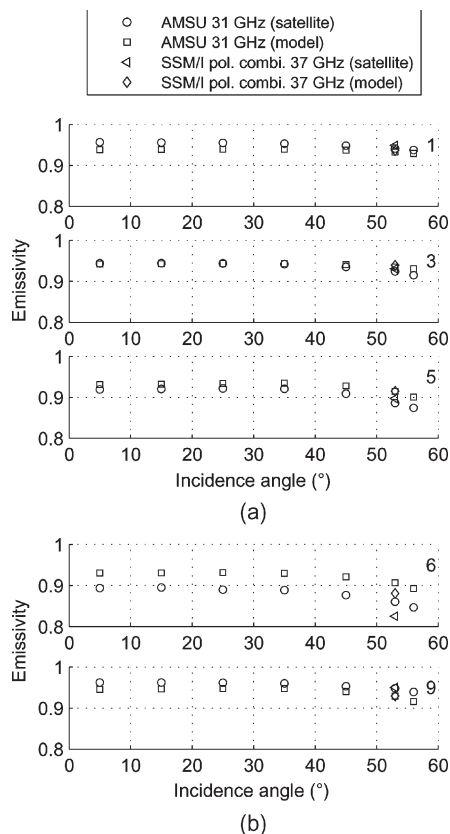
Fig. 7. Mean emissivity angular dependence as observed from satellite-derived emissivities from AMSU-A at 31 GHz and compared to the estimates at 37 GHz derived from SSM/I (a) for three snow-free surfaces and (b) for snow areas.
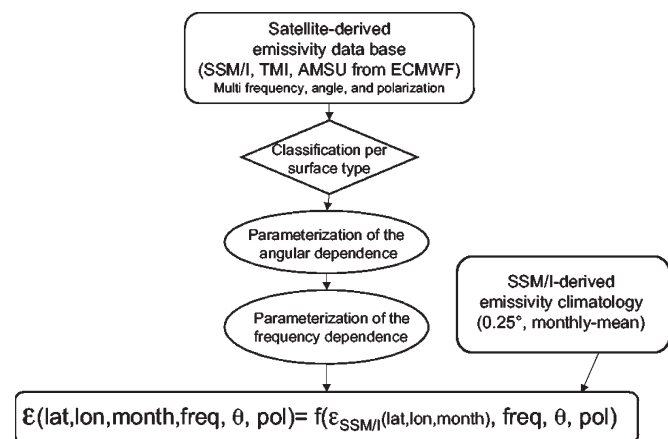

Fig. 8. Schematic presentation of the methodology.

satellite emissivities at 85 GHz. For all the surface types (snow-free and snow-covered regions), the angular dependence is smooth and limited: the polarization-combined AMSU emissivities are almost constant with the incidence angle up to 40° and then slightly decrease. The SSM/I- and TMI-derived emissivities around 53° at vertical and horizontal polarizations have been combined for comparison with the AMSU estimates. A rather good agreement is observed for all the surface types. Similar behaviors are seen at the other frequencies (not shown).

As compared to the model, the angular dependence of the satellite-derived emissivities is larger than the model ones
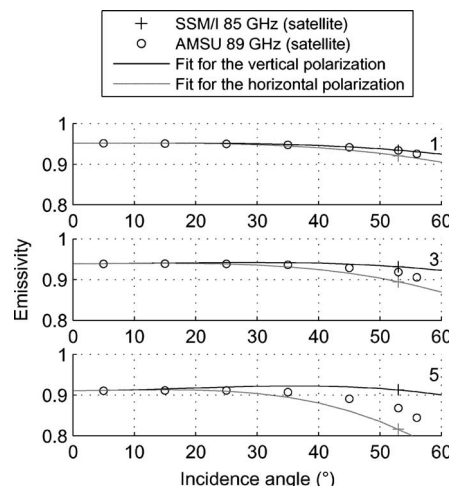

Fig. 9. Angular interpolation for each polarization, for three snow-free classes, as derived from the AMSU 89-GHz emissivities and anchored to the 85-GHz SSM/I emissivities.

(see Fig. 7 at 37 GHz; similar results are observed at the other frequencies). This is also related to the smaller polarization differences seen in the model than in the observation-derived emissivities.

IV. PARAMETERIZATION AND ITS RESULTS

Fig. 8 shows the methodology that is developed to derive the parameterization of the emissivity estimate for each location, month, frequency (between 19 and 100 GHz), incidence angle, and polarization. The development of the parameterization is based on the SSM/I and AMSU emissivity calculation performed at the ECMWF for January 2003, using only half the pixels for the snow-covered region. The method is then tested on the July 2002 emissivity calculations for the snow-free regions and on the remaining half of the January 2003 snow-covered pixels (as there is a very limited number of snow-covered pixels in July).

A. Parameterization of the Angular Dependence and Description of the Algorithm

1) Parameterization of the Angular Dependence: For each class that was previously defined, a polynomial function (third degree) is defined to describe the angular dependence of each polarization that fits both the SSM/I and AMSU-derived estimates. The polynomial function is calculated through a gradient descent to minimize the difference with the satellite-derived SSM/I and AMSU estimates. Fig. 9 shows the polynomial functions for three snow-free classes at 85 GHz, along with the corresponding satellite-derived emissivities from the SSM/I and AMSU.

2) Description of the Algorithm: The algorithm works as follows:

1) Selection of a location (latitude and longitude), month, frequency, and incidence angle. For a given location and month, a snow flag derived from the National Snow and Ice Data Center data is specified (snow or no snow).
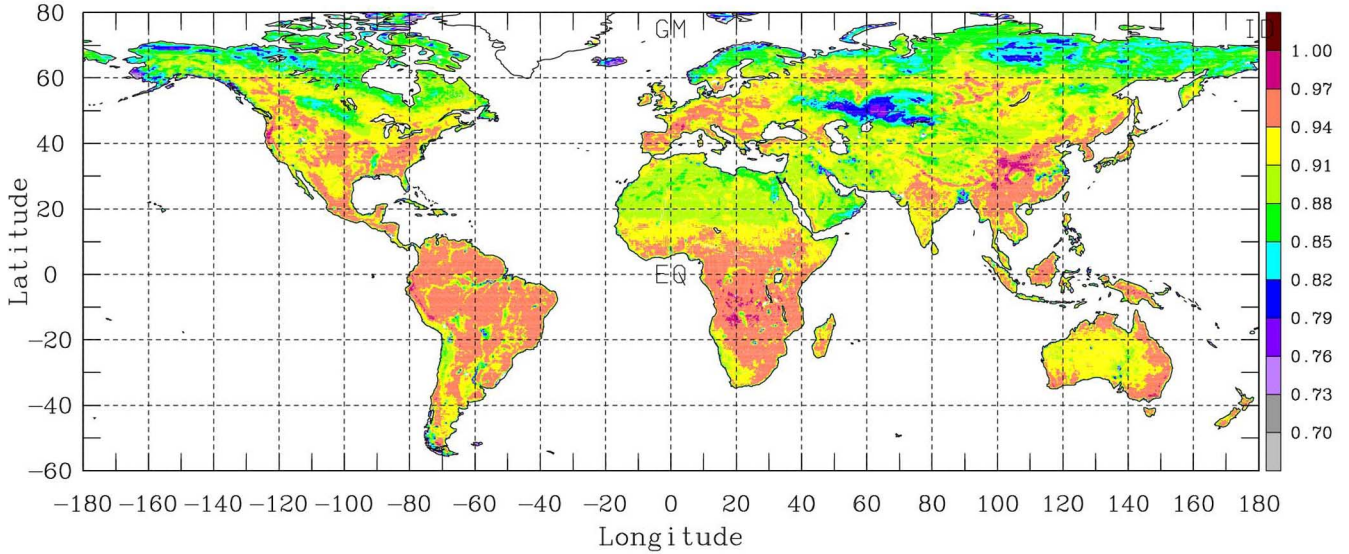
Fig. 10.   Example of an emissivity map at 30 GHz, for a 40° incidence angle, horizontal polarization in February.
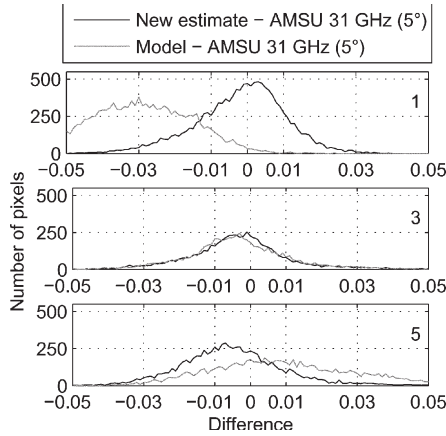

Fig. 11.   Histogram of the differences between the new interpolated emissivity and the satellite-derived emissivity, along with the difference between the modeled emissivity and the satellite-derived emissivity, at 31.4 GHz, 5° incidence angle, for AMSU-A for three snow-free classes.

2) Search in the SSM/I climatology database for the emissivities for that given location and month. It gives $e_v(53°)$ and $e_h(53°)$ for the SSM/I frequencies at 19.35, 37.0, and 85.5 GHz.

3) For each frequency (19.35, 37.0, and 85.5 GHz), calculation of the corresponding emissivity at nadir [$e_v(0°)$ and $e_h(0°)$] from a multilinear regression of $e_v(53°)$ and $e_h(53°)$. The coefficients of this multilinear regression have been calculated from each class, separately.

4) Application of the polynomial function that describes the angular dependence for each polarization and each SSM/I frequency to deduce the $e_v(\theta)$ and $e_h(\theta)$ emissivities.

5) Linear interpolation in frequency to derive $e_v(\theta)$ and $e_h(\theta)$ at the selected frequency from the three SSM/I frequency emissivity functions.

B. Results and Comparison With Other Estimates

Fig. 10 shows an example of parameterization at 30 GHz, at 40° incidence angle, horizontal polarization, for February.

The results of the parameterization are tested using the AMSU emissivities calculated at ECMWF for July 2002 and for half the pixels for January 2003 over snow. The ECMWF calculations are compared with both the parameterization results and the emissivity model outputs, which are also calculated at ECMWF (see Section II-B). The histograms of the differences for both estimates, at 31 GHz and 5° incidence angle, for the three snow-free classes are shown on Fig. 11. With the new parameterization over the snow-free regions, the differences are centered close to zero with a limited dispersion, regardless of the surface type. The behavior of the model is highly dependent on the surface type.

Table I summarizes the results of the comparison at 23, 31, and 89 GHz at 15° and 45° for each class. The bias is indicated, as well as the rms (in parentheses). Fig. 12 shows the rms error as a function of the surface class, for 15°, for both estimates.

For the snow-free regions, the new parameterization gives the rms values that are usually within 0.02, with a limited bias. Only a fraction of this error is directly related to the angular and frequency parameterization itself; the rest is due, first, to the temporal variabilities of the emissivities over a month and from year to year, and second, to the conditions of the calculation that were different at ECMWF and for the initial SSM/I emissivity climatology (Section II-A). The standard deviation of the emissivities within a month have been characterized [5] and are of the order of 0.01 at 19 GHz and can reach 0.02 at higher frequencies over snow (for the SSM/I emissivity database, these standard deviations are available along with monthly mean emissivities on our Web site geo.obspm.fr). The gaseous absorption model, the surface skin temperature, and the cloud detection schemes are different in the calculations performed at the ECMWF and for the initial SSM/I emissivity climatology, inducing potential differences between the calculated emissivities; the sensitivity of the calculation to these various factors have already been evaluated [5]. For classes 2 and 3, the rms errors of the model are also almost always below 0.03.

TABLE I
COMPARISON BETWEEN THE NEW PARAMETERIZATION AND THE SATELLITE-DERIVED EMISSIVITIES (A) AS WELL AS BETWEEN THE MODEL
ESTIMATES AND THE SATELLITE-DERIVED EMISSIVITIES (B) AT 23, 31, AND 89 GHz AT 15° AND 45° FOR EACH CLASS. THE BIAS IS
INDICATED, AS WELL AS THE RMS (BETWEEN PARENTHESES)

| Class	15° 23GHz	45° 23GHz	15° 31GHz	45° 31GHz	15° 89GHz	45° 89GHz
1 (a)	-.003(.014)	.003(.015)	-.003(.013)	.001(.014)	.006(.016)	.006(.018)
1 (b)	-.034(.037)	-.028(.033)	-.025(.029)	-.020(.026)	.003(.015)	.009(.020)
2 (a)	-.006(.017)	.002(.018)	-.005(.016)	.000(.017)	.003(.018)	.005(.020)
2 (b)	-.024(.028)	-.017(.024)	-.016(.021)	-.010(.018)	.009(.018)	.017(.024)
3 (a)	-.003(.016)	.006(.018)	-.002(.015)	.004(.017)	.007(.017)	.010(.021)
3 (b)	-.010(.019)	-.002(.019)	-.002(.015)	.005(.019)	.020(.030)	.027(.037)
4 (a)	-.003(.018)	.007(.021)	-.002(.017)	.005(.020)	.009(.020)	.014(.027)
4 (b)	.003(.022)	.013(.029)	.010(.024)	.019(.031)	.017(.044)	.028(.054)
5 (a)	-.003(.019)	.012(.022)	-.003(.017)	.007(.019)	.010(.021)	.017(.030)
5 (b)	.009(.028)	.019(.032)	.012(.028)	.020(.032)	-.033(.060)	-.023(.062)
6 (a)	-.006(.039)	.008(.037)	.001(.047)	.010(.042)	.046(.070)	.051(.070)
6 (b)	.013(.047)	.024(.049)	.029(.052)	.040(.060)	-.309(.402)	-.308(.399)
7 (a)	-.005(.027)	.007(.029)	.009(.032)	.011(.033)	.036(.066)	.041(.068)
7 (b)	-.017(.031)	-.006(.028)	-.001(.032)	.008(.036)	-.327(.415)	-.328(.417)
8 (a)	-.001(.023)	.008(.027)	.003(.025)	.004(.030)	.005(.071)	.007(.071)
8 (b)	-.021(.031)	-.015(.029)	-.010(.029)	-.005(.031)	-.180(.300)	-.188(.309)
9 (a)	-.004(.019)	.003(.020)	-.003(.021)	-.000(.023)	-.004(.061)	.001(.062)
9 (b)	-.030(.034)	-.027(.032)	-.018(.026)	-.016(.025)	-.080(.166)	-.089(.179)
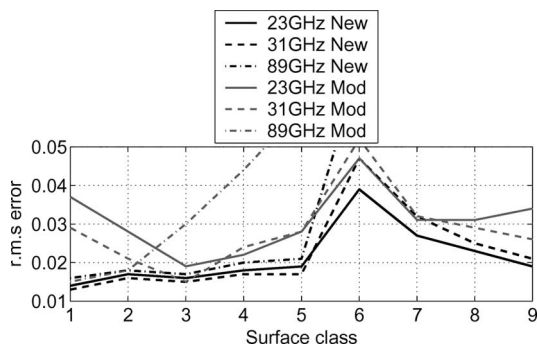
Fig. 12. RMS error between the new parameterization and the satellite-derived emissivities (black lines), as well as between the model estimates and the satellite-derived emissivities (gray lines) at 23, 31, and 89 GHz at 15° as a function of surface class.

For the snow-covered regions, much larger errors are observed, particularly at high frequencies for the snow classes that correspond to low emissivities (classes 6 and 7). In these regions, snow signatures are dominated by scattering, particularly at high frequencies, with a large temporal and spatial variability related to snow-grain metamorphism [20].

The emissivity model outputs have larger bias and rms for most cases. The ability of the model to represent the complexity of the radiation/surface interaction can be questioned. However, a large part of the error is likely related to the simplicity of the ECMWF surface model from which the emissivity model inputs are derived. This is particularly true over snow, where parameters like grain size distribution and stratification have a strong effect on the emissivity but are not available from the land surface models.

V. CONCLUSION

The angular and frequency dependences of the microwave land surface emissivities are analyzed between 10 and 90 GHz from estimates derived from SSM/I, TMI, and AMSU and are compared to model calculations. For a given surface type, both the angular and frequency dependences are rather limited and monotonic above 19 GHz. Below 19 GHz, the frequency dependence is different, and an additional work is to be performed, using Advanced Microwave Scanning Radiometer observations for instance. The general frequency and angular behaviors are rather similar, from models and satellite-derived emissivities, but differences in emissivities can be more than 10%.

From the analysis of the satellite-derived frequency and angular dependences, a parameterization is developed to estimate global microwave emissivities from the 19 to 100 GHz range for all the incidence angles and for both polarizations. It is anchored to a monthly mean emissivity climatology derived from the SSM/I observations for over a decade. The results are compared with model outputs and satellite estimates. The rms error is expected to be lower than 0.02 in snow-free region. The parameterization algorithm is available to the community, as well as the monthly mean emissivity climatology which it requires as inputs. The covariance of the emissivities from the original SSM/Iderived database is also accessible.

The uses of these emissivities are manifold as follows:

1) estimate the surface contribution in a cloud-clearing procedure;
2) as the first guess in the assimilation of close-to-the-surface sounding channels;
3) as the first guess in surface skin temperature retrievals using microwave observations for an "all-weather" estimate of the surface temperature to complement the infrared estimates that are only available under clear-sky condition;
4) evaluate the surface background contribution in precipitation and cloud retrievals;
5) simulate the responses of future instruments.

Efforts have to be conducted in collaboration with the land surface and emissivity modelers to better understand the differences observed between the satellite-derived and modeled emissivities. That will lead to the development of reliable and accurate emissivity models for global applications.

REFERENCES

[1] C. Matzler, "Passive microwave signatures of landscapes in winter," *Meteor. Atmos. Phys.*, vol. 54, no. 1–4, pp. 241–260, Mar. 1994.

[2] T. J. Hewison, "Airborne measurements of forest and agricultural land surface emissivity at millimeter wavelengths," *IEEE Trans. Geosci. Remote Sens.*, vol. 39, no. 2, pp. 393–399, Feb. 2001.

[3] J. Shi, K. S. Chen, Q. Li, T. J. Jackson, and P. E. O'Neil, "A parameterized surface reflectivity model and estimation of bare-surface soil moisture with L-band radiometer," *IEEE Trans. Geosci. Remote Sens.*, vol. 40, no. 12, pp. 2674–2686, Dec. 2002.

[4] F. Weng, B. Yan, and N. C. Grody, "A microwave land emissivity model," *J. Geophys. Res.*, vol. 106, no. D17, pp. 20 115–20 123, 2001.

[5] C. Prigent, W. B. Rossow, and E. Matthews, "Microwave land surface emissivities estimated from SSM/I observations," *J. Geophys. Res.*, vol. 102, no. D18, pp. 21 867–21 890, 1997.

[6] F. Karbou, C. Prigent, L. Eymard, and J. Pardo, "Microwave land emissivity calculations using AMSU measurements," *IEEE Trans. Geosci. Remote Sens.*, vol. 43, no. 5, pp. 948–959, May 2005.

[7] C. Prigent, F. Aires, and W. B. Rossow, "Land surface microwave emissivities over the globe for a decade," *Bull. Amer. Meteorol. Soc.*, vol. 87, no. 11, pp. 1573–1584, Nov. 2006. DOI:10.1175/BAMS-87-11-1573.

[8] T. Pellerin, J.-P. Wigneron, J.-C. Calvet, and P. Waldteufel, "Global soil moisture retrieval from a synthetic L-band brightness temperature data set," *J. Geophys. Res.*, vol. 108, no. D12, p. 4364, 2003. DOI:1.1029/2002JD003086.

[9] A. Wiesmann, C. Fierz, and C. Matzler, "Simulation of microwave emission from physically modeled snowpacks," *Ann. Glaciol.*, vol. 31, no. 1, pp. 397–405, Jan. 2000.

[10] C. Prigent, F. Chevallier, F. Karbou, P. Bauer, and G. Kelly, "AMSU—A land surface emissivity estimation for numerical weather prediction assimilation schemes," *J. Appl. Meteorol.*, vol. 44, no. 4, pp. 416–426, Apr. 2005.

[11] J. P. Hollinger, J. L. Pierce, and G. A. Poe, "SSM/I instrument evaluation," *IEEE Trans. Geosci. Remote Sens.*, vol. 28, no. 5, pp. 781–790, Sep. 1990.

[12] R. W. Saunders, "Note on the advanced microwave sounding unit," *Bull. Amer. Meteorol. Soc.*, vol. 74, pp. 2211–2212, 1993.

[13] W. B. Rossow and R. A. Schiffer, "Advances in understanding clouds from ISCCP," *Bull. Amer. Meteorol. Soc.*, vol. 80, no. 11, pp. 2261–2287, Nov. 1999.

[14] J. R. Eyre, "A fast radiative transfer model for satellite sounding systems," ECMWF, Reading, U.K., p. 1991, ECMWF Tech. Memo. 176.

[15] R. Saunders, M. Matricardi, and P. Brunel, "An improved fast radiative transfer model for assimilation of satellite radiance observations," *Q. J. R. Meteorol. Soc.*, vol. 125, no. 556, pp. 1407–1425, Apr. 1999.

[16] E. Kalnay *et al.*, "The NCEP/NCAR 40-year reanalysis project," *Bull. Amer. Meteorol. Soc.*, vol. 77, no. 3, pp. 437–470, Mar. 1996.

[17] T. Kohonen, *Self-Organization and Associative Memory*. New York: Springer-Verlag, 1984.

[18] C. Prigent, F. Aires, W. B. Rossow, and E. Matthews, "Joint characterization of vegetation by satellite observations from visible to microwave wavelength: A sensitivity analysis," *J. Geophys. Res.*, vol. 106, no. D18, pp. 20 665–20 685, 2001.

[19] C. Prigent, F. Papa, F. Aires, W. B. Rossow, and E. Matthews, "Global inundation dynamics inferred from multiple satellite observations, 1993–2000," *J. Geophys. Res.*, vol. 112, D12107, 2007.

[20] E. Cordisco, C. Prigent, and F. Aires, "Snow characterization at a global scale with passive microwave satellite observations," *J. Geophys. Res.*, vol. 111, no. D19, D19102, 2006. DOI:10.1029/2005JD006773.

Catherine Prigent received the Ph.D. degree in physics from Paris University, Paris, France, in 1988.

Since 1990, she has been a Researcher with the Laboratoire d'Etudes du Rayonnement et de la Matière en Astrophysique, Paris Observatory, Centre National de la Recherche Scientifique (CNRS), Paris, France. From 1995 to 2000, she was on leave from CNRS and worked at the NASA Goddard Institute for Space Studies, Columbia University, New York, NY. Her research interests focus on passive microwave remote sensing of the Earth. Her early work focused on the modeling of the sea surface emissivities at microwave wavelengths and the estimation of atmospheric parameters over the ocean from microwave measurements. Currently, her main interests include the calculation and analysis of microwave land surface emissivities, estimation of atmospheric and surface parameters over land from microwave observations, as well as multisatellite characterization of the land surface. She is also involved in satellite remote sensing of clouds with the analysis of passive-microwave observations over convective cloud structures.

Elodie Jaumouillé received the M.S. degree in applied mathematics from Bordeaux I University, Bordeaux, France, in 2005. She is currently working toward the Ph.D. degree in applied mathematics at Cemagref, Bordeaux.

She was with the Laboratoire des Sciences du Climat et de l'Environnement, Commissariat à l'Énergie Atomique, Gif-Sur-Yvette Cedex, France, where she was involved in the numerical and scientific validation of several climate models' outputs. Then, she is with the Laboratoire d'Etudes du Rayonnement et de la Matière en Astrophysique, Paris Observatory, Paris, France. She studied the frequency and angular variations of microwave emissivities. She is investigating how to control the hydraulic state of a drinkable-water network in order to minimize losses and to assure a better quality for the customer.

Frédéric Chevallier received the M.S. degree in physics at the University of Rennes, Rennes, France, in 1993. His Ph.D. work, which he defended in 1998, consisted of the development of a neural-network-based infrared radiation model for use in general circulation models. This study took place at the Laboratoire de Météorologie Dynamique, Palaiseau Cedex, France.

In 1998, he was with the European Centre for Medium Range Weather Forecasts, Reading, U.K., to work in the physical aspects and satellite sections. There he adapted his radiation model, which was made operational in 2003 as part of the 4-D-Var physics. His involvement in the data assimilation system increased over the years, particularly in initiating the assimilation of cloud-affected and rain-affected satellite radiances. He was appointed as a Permanent Research Scientist with the Laboratoire des Sciences du Climat et de l'Environnement, Gif-Sur-Yvette Cedex, France, in December 2003. His current research interests focus on the Bayesian inversion of the surface fluxes of atmospheric compounds from *in situ* and remote sensing atmospheric measurements.

Filipe Aires received the Ph.D. degree in statistics from the University Paris–Dauphine, Paris, France, in 1999.

He was with the NASA Goddard Institute for Space Studies, New York, NY, for five years, and he is now a Research Scientist with the Laboratoire de Météorologie Dynamique, Centre National de la Recherche Scientifique, Palaiseau Cedex, France. His research interests focus on satellite remote sensing of the Earth and statistical analysis of the climate. In earlier works, he analyzed climatic signals, using statistical techniques such as independent component analysis. He has also defined new tools for the characterization of climate feedback. He has developed multiinstrument and multiparameter remote sensing algorithms to retrieve atmospheric variables such as temperature, ozone, or water vapor profiles, and surface variables such as surface skin temperature, vegetation indices, or microwave emissivities. Instruments involved in these remote sensing studies include Advanced Microwave Sounder Unit, Special Sensor Microwave/Imager, Infrared Atmospheric Sounding Interferometer, European Remote-Sensing, and TIROS Operational Vertical Sounder. Currently, he is involved in the development of remote sensing algorithms for the French–Indian mission Megha-Tropiques.